JOURNAL OF APPLIED ELECTROCHEMISTRY **26** (1996) 775–784

Voltammetry in the presence of ultrasound: mass transport effects

R. G. COMPTON*, J. C. EKLUND, S. D. PAGE

Physical Chemistry Laboratory, Oxford University, South Parks Road, Oxford, OX1 3QZ, Great Britain

T. J. MASON, D. J. WALTON

School of Natural and Environmental Sciences, Coventry University, Priory Street, Coventry, CV1 5FB, Great Britain

Received 15 August 1995; revised 23 October 1995

The voltammetry of various well-defined systems in acetonitrile solution has been studied using both micro and macroelectrodes in the presence of power ultrasound. A simple model is established which quantifies the mass transport observed under these conditions; this assumes that the effect of ultrasound is to promote mixing within the bulk of the solution up to within a certain distance of the electrode surface. Thus the ultrasound serves to thin the diffusion layer which would exist at the corresponding electrode under silent conditions. The relative enhancement of transport limited currents by ultrasound is dependent on the size of the electrode; for micrometre-sized electrodes the steady state limiting current observed tends to that predicted under silent conditions whereas for large electrodes a thin, steady-state diffusion layer is seen with a thickness which is power dependent. In addition to steady-state experiments, a.c. impedance measurements and potentials steps are used to verify the model proposed.

1. Introduction

Various workers have reported beneficial results from exposing electrochemical cells to the effects of power ultrasound. Areas of application include electroplating [1, 2], the deposition of polymer films [3, 4] and electrosynthesis [5]. Several physical mechanisms exist by which ultrasound might modify electrode processes including the formation of ions, radicals and other high energy intermediates during transient cavitation, the ultrasonic mediation of chemical processes associated with electron transfer steps, continuous cleaning and activation of the electrode surface, and the enhanced rate of mass transport resulting from cavitation in solution [6, 7]. It is this last aspect which the present paper seeks to address through the validation of a mathematical model for the rate of mass transport in the presence of ultrasound. In particular we make use of a well-thermostatted cell of the construction shown in Fig. 1 in which an ultrasonic horn is immersed in the solution of interest at a known distance, d, above an electrode of a chosen (variable) radius ranging from 2.5 μm to 0.4 cm. This is used to study the voltammetric characteristics of several well-defined simple one electron oxidations and reductions in acetonitrile solution. The experimental results are reported after a mathematical model is developed in the following section. Subsequent papers will address the other physical effects of ultrasound on electrode processes identified above.

2. Theory

We consider the simple one electron process:

$$A \pm e^- \rightleftharpoons B$$

and examine first the mass transport limited current flowing at a microdisc electrode achieved through applying a potential step to the electrode at time $t = 0$ so that the potential changes from a value at which no current flows to one at which the mass transport limited current is established. The time-dependent transport equation is

$$\frac{\partial a}{\partial t} = D\frac{\partial^2 a}{\partial z^2} + D\frac{\partial^2 a}{\partial r^2} + \frac{D}{r}\frac{\partial a}{\partial r} \qquad (1)$$

where r and z are defined in Fig. 2, $a = [A]$ and D is the diffusion coefficient of A. In the absence of ultrasound then the boundary conditions corresponding to the problem of interest are as follows where r_e is the electrode radius,

for $t > 0$:	$z = 0$	$0 < r < r_e$	$a = 0$
	$z = 0$	$r > r_e$	$\frac{\partial a}{\partial z} = 0$
	all r	$z \longrightarrow +\infty$	$a = a_{bulk}$
	all z	$r \longrightarrow +\infty$	$a = a_{bulk}$
for $t < 0$:		all r, all z	$a = a_{bulk}$

The form of the chronoamperometric transient

* Author to whom correspondence should be sent.

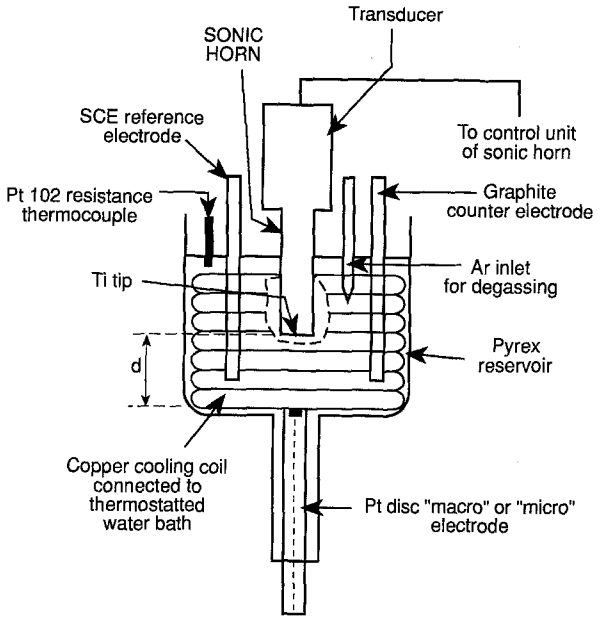

Fig. 1. Sonoelectrochemical cell used for the voltammetric studies.

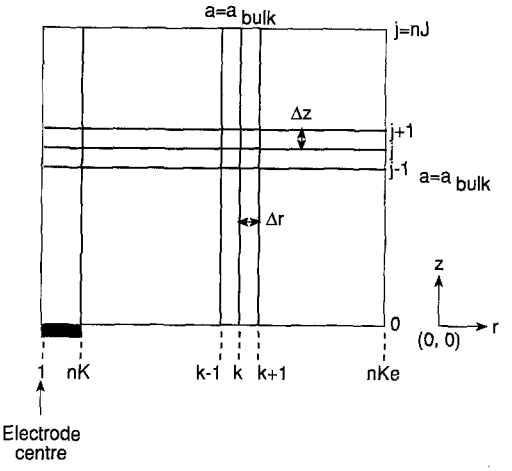

Fig. 2. Cylindrical coordinates used to describe mass transport to a microdisc electrode. Also shown is the finite difference grid used in the Hopscotch computations described where nKe is the total number of points in the r direction, nJ is the total number of points in the z direction, nK is the total number of points over the electrode. Δr is the separation between points in the finite difference grid in the r direction, and Δz is the equivalent separation in the z direction.

resulting from the potential step is well known [8, 9] and a steady state current of magnitude [10]

$$I = 4nFDa_{\text{bulk}}r_e \qquad (2)$$

is established. This equation implies an average diffusion layer [10] thickness over the electrode of size $\pi r_e/4$ although as a result of the non-uniform current density on the electrode the diffusion layer will be thinnest at the electrode edges and fattest at the electrode centre. In the presence of ultrasound we suppose that the effect of cavitation in solution is to promote mixing in the solution close to the electrode so that the diffusion layer thickness cannot exceed a maximum value z^* controlled by the incident power level. This is schematically illustrated in Fig. 3. For this situation the above boundary conditions are modified as follows:

for $t > 0$:	$z = 0$	$0 < r < r_e$	$a = 0$
	$z = 0$	$r > r_e$	$\dfrac{\partial a}{\partial z} = 0$
	all r	$z > z^*$	$a = a_{\text{bulk}}$
	all z	$r \longrightarrow +\infty$	$a = a_{\text{bulk}}$
for $t < 0$:		all r, all z	$a = a_{\text{bulk}}$

where z^* is the thickness of the truncated diffusion layer. The form of the chronoamperometric transient resulting under these conditions was explored using the hopscotch algorithm [9, 11] to facilitate the numerical integration of Equation 1 subject to these boundary conditions. The basis of this approach has been described elsewhere [11] for the case of mass transport to microband electrodes; no new conceptual or computational problems emerge in the present application. Accordingly the reader is directed to the literature [8, 9, 11] for full details of the necessary procedure. In this manner the concentration of A near the sonicated microelectrode was explored and the current (I)/time transients evaluated using the following expression

$$I = 2\pi FD\int_0^{r_e}\left(\frac{\partial a}{\partial z}\right)_{z=0} r\,dr$$

where F is the Faraday constant, for different values of r_e and z^*.

We turn next to consideration of the diffusion layer under conditions of ultrasonically enhanced mass transport at a macroelectrode. The natural extension of the model described above for microelectrodes is to assume a diffusion layer of uniform thickness, z^*, across the electrode surface, 'edge' effects being rendered negligible by virtue of the large size of the electrode. Under these conditions a steady state current is observed of magnitude

$$I = D\pi r_e^2 F a_{\text{bulk}}/z^* \qquad (3)$$

3. Theoretical results and discussion

First the numerical strategy outlined above was verified by calculating the transient current due to a potential step in the absence of ultrasound for microdisc electrodes of two different sizes: 13.6 and 30 μm. A concentration of 1.0×10^{-3} mol dm^{-3} and a diffusion coefficient of 1.0×10^{-5} cm^2 s^{-1} were assumed. The following parameters were used in the computation [11, 12] to ensure convergence to better than

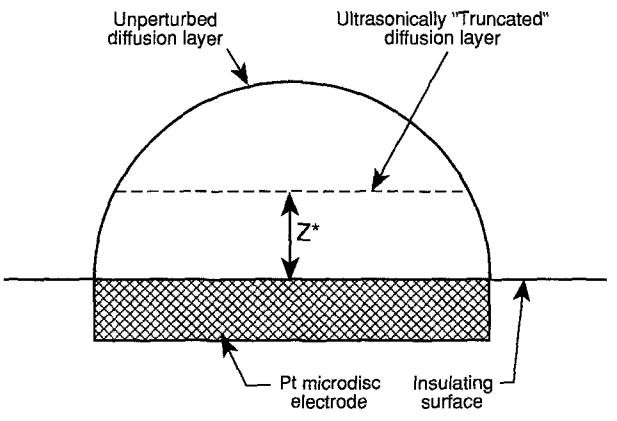

Fig. 3. Postulated thinning of the diffusion layer caused by ultrasonically induced cavitation in solution.

1% in the steady-state current: time increment $\Delta t = 1 \times 10^{-5}$ s, number of grid points in the r-direction over the electrode surface $(nK) = 40$, total number of grid points in the r-direction $(nKe) = 800$, total number of grid points in the z-direction $(nJ) = 500$ such that the distances between the points $\Delta r = \Delta z = r_e/39$ (see Fig. 2). Figure 4 shows the two computed transients together with the corresponding theoretical transients calculated from the expression derived by Heinze [13]:

$$I(t) = nFAa_{\text{bulk}}\left(\frac{D}{t\pi}\right)^{1/2}\left[1 + b\left(\frac{Dt}{r_e^2}\right)^{1/2}\right] \quad (4)$$

where t is the time and A is the electrode area. A value of 2.00 for the coefficient b was used [13]. Good agreement between theory and experiment is evident in Fig. 4 and in both cases the steady-state current established at long times was found to be in quantitative agreement with Equation 2.

Attention was next turned to the computation of current transients for the case of the ultrasonically truncated diffusion layer. In these computations the previous constraint that $\Delta r = \Delta z$ was relaxed in the interests of accurate computation; again $\Delta r = r_e/39$ but Δz was varied such that $\Delta z = z^*/nJ$ (see Fig. 2) and Δt reduced appropriately (see below). Values of nJ of 600 to 1000 were found to give convergence of the steady-state current to within 1%. Figure 5 shows the computed transients for a microdisc electrode of radius 30 μm with $z^* = 3.24\,\mu$m and 10 μm. The diffusion coefficient and electrolyte concentrations used were as above. The transients were calculated using values of $\Delta t = 3.33 \times 10^{-8}$ s and 3.33×10^{-7} s, respectively. Notice that the timescale of these transients are both more rapid than the corresponding 'silent' transient shown in Fig. 4(b). Also the smaller the value of z^* the faster the timescale of the transient and the larger the steady-state limiting current.

4. Experimental details

Three separate horns were employed in this work. These were supplied by Heat Systems (model W380) and Sonics & Materials (models VC385 and VCX400) and had titanium tipped horn probes (of diameter 13 mm) extended by 127 mm and operating at 20 kHz. Power levels up to and including 63 W cm^{-2} were employed and calibrated calorimetrically. Thermostatting of the electrochemical cell was accomplished by means of a copper cooling coil inserted in the solution through which water was circulated from a constant temperature bath. By

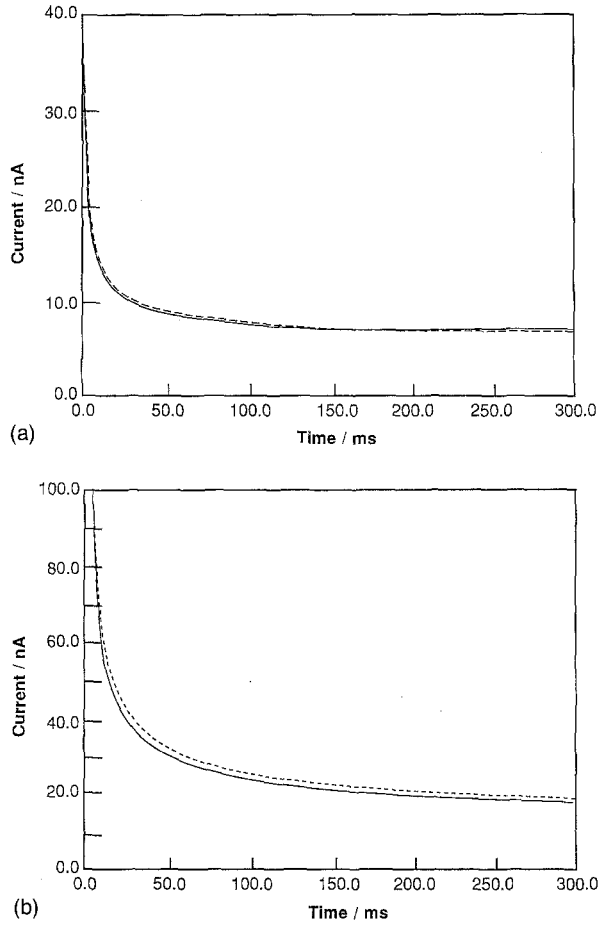

Fig. 4. Current transients resulting from potential steps at microdisc electrodes of radius, r_e: (a) 13.6 μm and (b) 30.0 μm. The solid line shows the results of the Hopscotch computations and the dashed line the transient calculated from the analytical expression given in the text [7].

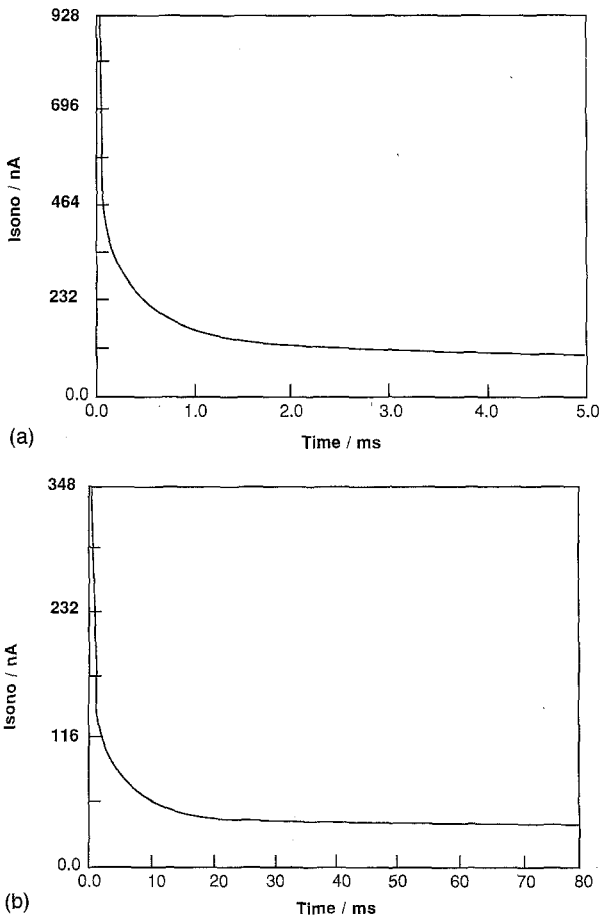

Fig. 5. Computed current transients resulting from potential steps at a microdisc electrode of radius, $r_e = 30.0\,\mu$m for the cases of truncated diffusion layer thicknesses of size $z^* = 3.24\,\mu$m (a) and z^* 10 μm (b).

limitation of the sonication time to less than one minute this arrangement enabled the voltammetric measurements to be conducted at constant temperature (estimated as within 2 °C).

Platinum microdisc electrodes were obtained from Bioanalytical Systems (West Lafayette, USA) and had radii of 2.5, 5.1, 13.6, 29.0 and 60.0 μm as measured electrochemically under steady state conditions. Macroelectrodes of radii 0.05, 0.1, 0.15, 0.21 and 0.39 cm were mounted in an insulating Teflon sheath. All electrodes were carefully polished before using diamond lapping compounds (Kemet, Kent, UK) of decreasing size down to 0.25 μm.

Voltammetric and a.c. impedance measurements were carried out using a Solatron 1286 electrochemical interface (in combination with a 1250 frequency response analyser for a.c. measurements) three-electrode potentiostat under computer control or an Oxford electrodes potentiostat. A carbon rod served as a counter electrode and a saturated calomel electrode completed the circuit as shown in Fig. 1.

The solvent used throughout was dried [14] acetonitrile (Fisons, dried, distilled), and tetrabutylammonium perchlorate (TBAP, Kodak, puris) served as the background electrolyte. Ferrocene, p-chloranil and tris(*p*-bromophenyl)amine were used as received from Aldrich (99%). $TBA_4^+[S_2Mo_{18}O_{62}]^{4-}$ and $[(\eta^5\text{-}C_5H_5)Fe(CO)(PPh_3)=C(NHMe)Me]BF_4$ were generous gifts from Professor A. Bond [15] and Dr S. G. Davies [16], respectively. No indications were observed for the sonochemical decomposition of any of the substrates under the conditions employed. Solutions were thoroughly purged of oxygen by bubbling through the solution argon that had been dried with calcium chloride and then presaturated with acetonitrile.

Supporting theory was generated from programs written in Fortran 77 using double precision on a Sun IPC workstation.

5. Results and discussion

Experiments were initially conducted using the one-electron oxidation of ferrocene in acetonitrile/0.1 M TBAP as a model and well-defined voltammetric system:

$$Cp_2Fe - e^- \rightleftharpoons Cp_2Fe^+ \quad E_{1/2} = +0.37\,V \text{ vs SCE [17]} \tag{5}$$

Figure 6 shows voltammograms obtained in the absence of ultrasound at disc electrodes of radius 13.6 μm and 0.10 cm, respectively ($a_{bulk} = 2.0 \times 10^{-3}$ mol dm^{-3}). The former has the characteristic sigmoidal shape expected from a microdisc electrode [18]. In contrast the macroelectrode displays the cyclic voltammogram expected for a reversible one-electron oxidation. In both cases the current/voltage waveshapes and magnitudes were consistent with the simple reversible process of Equation 5 and

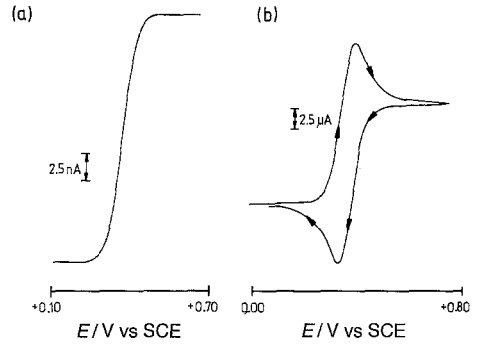

Fig. 6. Voltammograms recorded in the absence of ultrasound for the oxidation of Cp_2Fe (2.0 mM) in acetonitrile/0.1 M TBAP for (a) a microdisc electrode of radius 13.6 μm and (b) a macroelectrode of radius 0.1 cm. In the latter case a voltage sweep rate of 20 mV s^{-1} was used.

a value of $D = 2.3 \times 10^{-5}$ cm^2 s^{-1} for the diffusion coefficient of ferrocene [17].

We consider next the voltammetric behaviour in the presence of ultrasound. Figure 7 shows measurements analogous to those given in Fig. 6 except that 20 kHz ultrasound of intensity 44 ± 5 W cm^{-2} has been directed at the electrode surface using the experimental arrangement shown in Fig. 1 with a horn-electrode separation of 42 mm. For the case of the microelectrode the mean transport limited current is somewhat enhanced as compared to the silent case (Fig. 6(a)) but the form of the voltammogram is otherwise unaltered except for the presence of 'noise' superimposed on the voltammetric wave (as discussed below). In contrast the macroelectrode response is qualitatively changed from that of a familiar cyclic voltammogram to a sigmoidal shape indicative of a constant rate of transport of the electroactive species to the electrode surface so as to sustain a steady current. Again 'noise' was found to be imposed on the basic form of the voltammogram. The magnitude of the current in the macroelectrode case is considerably greater than that of the peak current seen under silent conditions and would correspond to a rotation speed of approximately 200 Hz were the electrode rotated in the absence of ultrasound to achieve an equivalent steady-state current!

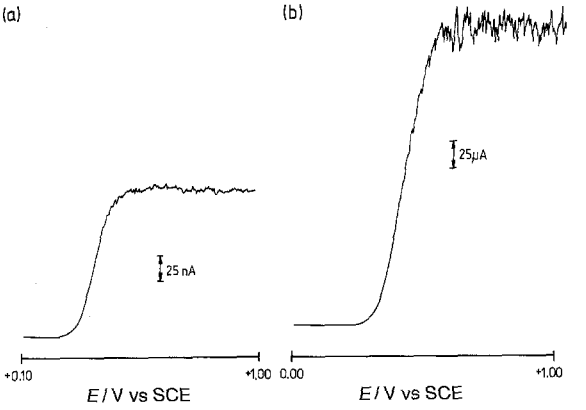

Fig. 7. Voltammograms recorded in the presence of ultrasound (20 kHz; intensity 44 ± 5 W cm^{-2} for the oxidation of Cp_2Fe (2.0 mM) in acetonitrile/0.1 M TBAP for (a) a microdisc electrode of radius 13.6 μm, and (b) a macroelectrode of radius 0.1 cm.

We have noted that both of the voltammograms shown in Fig. 7 display a significant noise component. This was recorded using a fast oscilloscope and shown to have a significant component very close to 20 kHz corresponding to the nominal frequency of the ultrasound employed. (Note that if the voltammograms are recorded using a chart recorder or slow digital system then this feature will become distorted). However, some 20 kHz a.c. signal was also observed when measurements were made in the absence of the electroactive substrate and at potentials cathodic of those required to bring about the oxidation of ferrocene. It was found that the magnitude of the a.c. component was much lower, and in fact almost disappeared, in the absence of supporting electrolyte. Specifically the 20 kHz a.c. component in pure acetonitrile was less than 0.4% of the magnitude of the corresponding signal observed in the presence of 0.1 M TBAP.

Experiments were then carried out on solutions of TBAP/acetonitrile to further investigate the nature of the a.c. component of the current. As might be expected from the turbulent conditions induced in bulk solution by ultrasonic agitation the magnitude of the ac component of the current was found to be difficult to precisely reproduce. However, approximate conclusions could be made from the data that was obtained. Initially the potential at the electrode was varied from a highly oxidative value to a highly reductive value and the amplitude and mean value of the a.c. current measured. The mean was found to change from a reductive current at negative potentials to an oxidative current at positive potentials. The switch over occurred at approximately +0.3 V vs SCE. The magnitude of the current was also found to vary as a function of potential and a minimum was observed again near $+0.3 \pm 0.15$ V vs SCE (see Fig. 8(a) which relates to a TBAP concentration of 50 mM). Both these observations were found to be the case for all concentrations of supporting electrolyte (TBAP) utilized in the range 0–100 mM. To investigate further the nature of this behaviour the variation of the interfacial capacitance with potential of the TBAP/acetonitrile/Pt interface, under silent conditions, was measured using a.c. impedance spectroscopy. A minimum for the interfacial capacitance was found, for all the concentrations of TBAP utilized, at a potential of $+0.3 \pm 0.1$ V vs SCE (see Fig. 8(b) which again corresponds to a concentration of 50 mM). We suggest that this is the potential of zero charge, E_{pzc}. It follows that E_{pzc} corresponds to both the minimum in the magnitude of the ac component of the current and the switch over potential reported above. Moreover, Fig. 8(c) shows a linear correlation between the current magnitude and the interfacial capacitance. Next the magnitude of the a.c. component was investigated as a function of the electrode area (see Fig. 9 which was measured using 50 mM TBAP). An approximately linear correlation was observed between the a.c. component magnitude and the area of the macroelectrodes. Corresponding

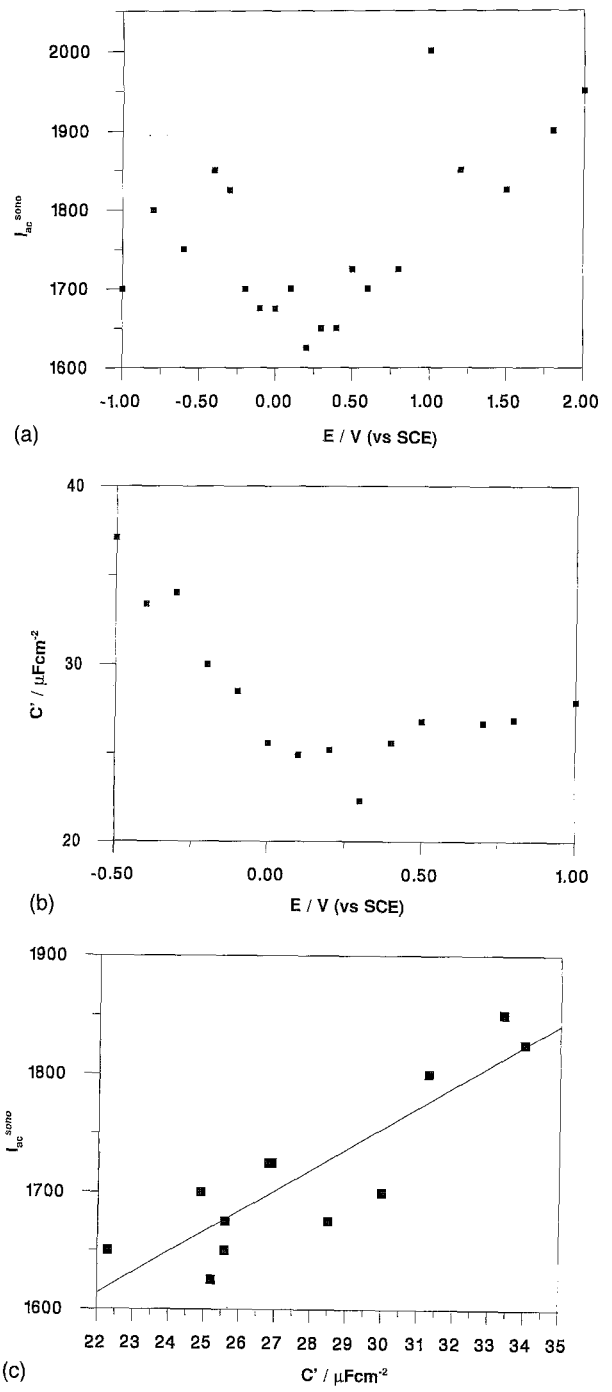

Fig. 8. Variation of (a) the magnitude of I_{ac}^{sono} and (b) the interfacial capacitance as a function of the electrode potential for a Pt disc electrode (radius 0.3 cm) in the presence of 5×10^{-2} mol dm^{-3} TBAP/acetonitrile; (c) shows that a linear correlation exists between the I_{ac}^{sono} and the interfacial capacitance.

observations were also made for other supporting electrolytes namely $LiClO_4$ and TBABr. This enabled us to discount the possibility that the ac component could be attributed to sonically induced decomposition of TBAP in acetonitrile.

The behaviour of the a.c. current may be rationalized as follows. The charge, q, dropped across the double layer at the electrode solution interface is related to the electrode area, A, the capacitance per unit area of the interface, C', and the drop in potential across the double layer, $\Delta\phi$:

$$q = AC'\Delta\phi$$

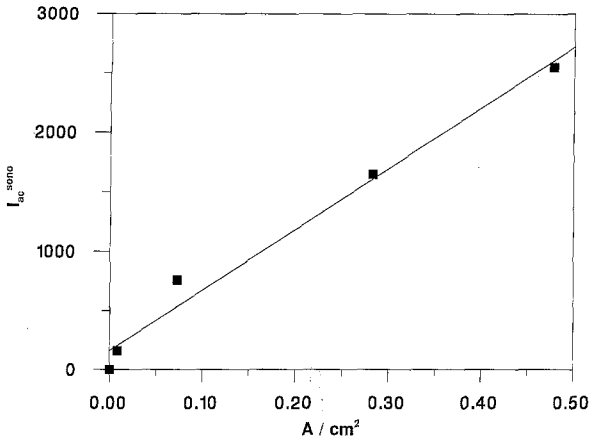

Fig. 9. Plot of I_{ac}^{sono} as a function of the electrode area, for a Pt macroelectrode 5×10^{-2} mol dm^{-3} TBAP/acetonitrile for an electrode potential of 0.0 V vs SCE.

Differentiation with respect to time gives

$$I = C'\Delta\phi\frac{dA}{dt} + C'A\frac{d\Delta\phi}{dt} + A\Delta\phi\frac{dC'}{dt}$$

Under (suitably fast) potentiostatic control the second term is zero. We suggest first that the ultrasonic waves arriving at the electrode surface induce a periodic compression of the double layer at a frequency of 20 kHz which is reflected in the term (dC'/dt); such behaviour has been characterized at lower frequencies [19].

We return to the voltammetric responses shown in Fig. 7 and examine, in greater detail, the nature of the d.c. component obtained after removal of the mean a.c. component discussed above. We consider first the effect of altering the distance, d, between the horn tip and the electrode surface. Figure 10 shows that as the separation is increased the current falls sharply to a steady value which is obtained for $d > 40$ mm. The latter value corresponds to approximately half the wavelength of sound in acetonitrile [20] and the fall-off distance was found to be independent of electrode size (2.5 μm to 0.39 cm).

Subsequent measurements were conducted with horn/electrode separations corresponding to the plateau region and these experiments were used to assess the mass transport models proposed in the theory section above. We turn first to results obtained for macroelectrodes of radius between 0.05 and 0.39 cm using a fixed incident ultrasonic power of 44 W cm^{-2}. The applicability of Equation 3 was tested by conducting experiments with variable concentrations of ferrocene, tris(*p*-bromophenyl)amine and *p*-chloranil. The first system has been discussed above and the second system is a well characterized simple one-electron oxidation [21]

$$(\text{Br-}\phi\text{-})_3\text{N} - e^- \rightleftharpoons (\text{Br-}\phi\text{-})_3\text{N}^+$$

$$E_{1/2} = +1.05\text{ V vs SCE [21]}$$

The third corresponds to the reduction [22]

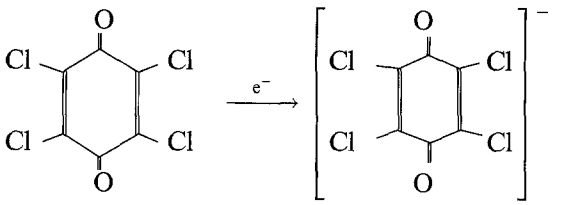

for which $E_{1/2} = +0.01$ V vs SCE. The diffusion coefficients for these two new systems were found to be 1.45×10^{-5} cm^2 s^{-1} and 1.80×10^{-5} cm^2 s^{-1}, respectively, as determined from independent rotating disc experiments.

Figure 11 shows that for electrodes of fixed area the d.c. current is directly proportional to the concentration of the electroactive species and this was found to be the case for all macroelectrodes studied. Note that the slopes of the three lines in Fig. 11 differ and this reflects the relative diffusion coefficients of the three species concerned (see below). Figure 12 shows that for a fixed concentration of depolarizer the magnitude of the d.c. current almost scales with electrode area suggesting a fixed diffusion layer thickness nearly independent of the electrode radius. This is quantified in Table 1 in which values of z^* inferred from Equation 3 are tabulated. It can be seen that as the electrode increases in size a constant diffusion layer thickness is established. Figure 13 shows that

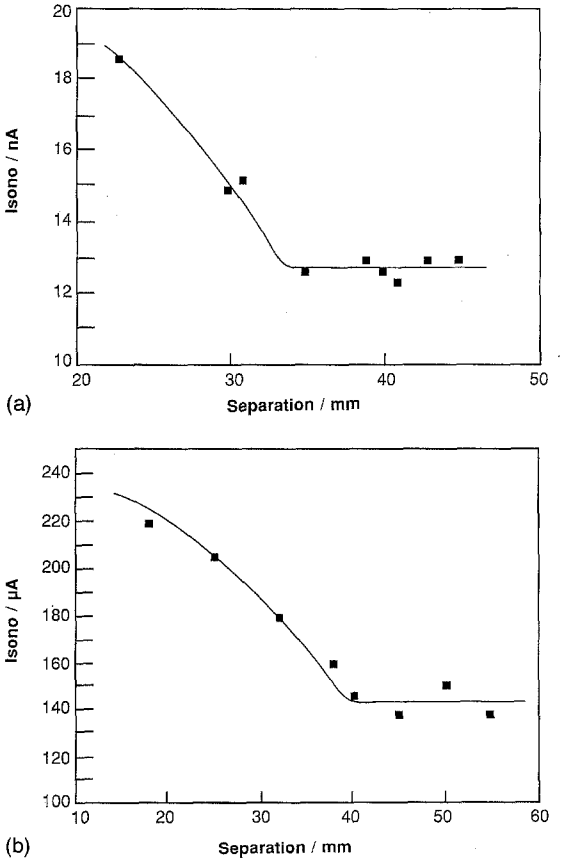

Fig. 10. Plot showing the influence of the electrode/horn separation, d, on magnitude of the d.c. current seen at the working electrode for (a) a microdisc of radius 5.1 μm and (b) a macroelectrode of radius 0.1 cm. In both cases a solution containing 10^{-3} M Cp_2Fe was used.

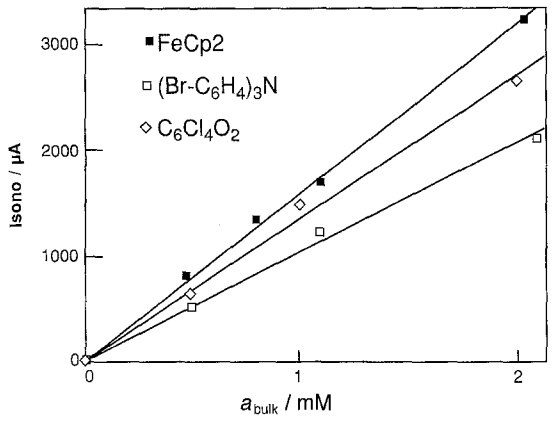

Fig. 11. Dependence of the steady d.c. current on the concentration of electroactive species obtained at an electrode of size 0.39 cm for each of the three systems studied.

for a fixed electrode size and constant concentration of electroactive species the current is directly proportional to the diffusion coefficient of the active species.

Further measurements were made using macroelectrodes as above but which employed variable levels of incident ultrasonic power. Equation 3 was used to infer values of the diffusion layer thickness, z^*, as a function of this incident power (p). Figure 14 shows the inferred relationship from which it can be seen that, as would be anticipated greater power causes increased mass transport due to enhanced cavitation leading to a greater thinning of the diffusion layer and thus a reduced value of z^*. It was found that the diffusion layer thickness correlated empirically with $p^{-0.6}$.

We next turn to the voltammetric measurements made using microelectrodes of radii between 2.5 and 60 μm. For all electroactive substrates studied the steady state current was found to be directly proportional to the concentration for a fixed electrode radius (and therefore z^*). Experiments were also undertaken to see if, with a fixed diffusion layer thickness, the current was directly proportional to the diffusion coefficient of the species discharging at the electrode surface as predicted by the truncated diffusion layer model given above. For this purpose

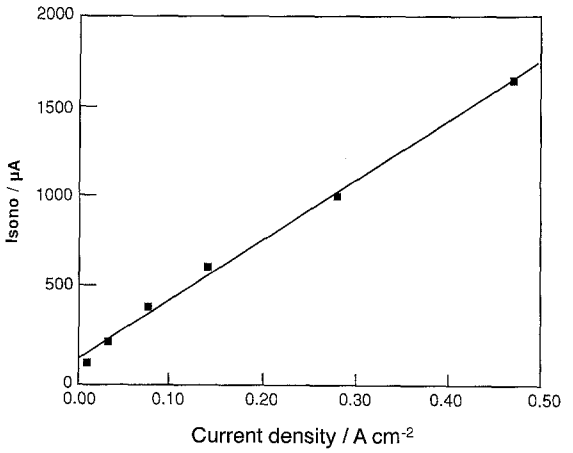

Fig. 12. Plot of d.c. current against electrode area obtained for macroelectrodes of different radius using 10^{-3} M Cp_2Fe and a ultrasonic power of 44 W cm^{-2}.

Table 1. The macroelectrode diffusion layer thickness as a function of electrode radius

Electrode radius/cm	z^*/μm
0.05	5.7 ± 0.7
0.10	5.6 ± 1.0
0.15	5.8 ± 0.7
0.21	6.3 ± 0.6
0.30	6.5 ± 0.7
0.39	6.5 ± 0.7

two systems additional to the three employed in the work described above were adopted. These were the one-electron oxidation of $[(\eta^5\text{-}C_5H_5)Fe(CO)(PPh_3)=C(NHMe)Me]BF_4$ [16]

$$[(\eta^5\text{-}C_5H_5)Fe(CO)(PPh_3)=C(NHMe)\,Me]^+ \rightleftharpoons [(\eta^5\text{-}C_5H_5)Fe(CO)(PPh_3)=C(NHMe)\,Me]^{2+} + e^-$$

$$E_{1/2} = +1.1\text{ V vs SCE}$$

and the one-electron reduction of $TBA_4[S_2Mo_{18}O_{62}]$ [15]

$$e^- + [S_2Mo_{18}O_{62}]^{4-} \rightleftharpoons [S_2Mo_{18}O_{62}]^{5-}$$

$$E_{1/2} = +0.49\text{ V vs SCE}$$

Both of these systems are known to be free from the complications of coupled homogeneous chemistry [15, 16]. Figure 15 shows that the predicted direct proportionality is observed.

Next the validity of the truncated diffusion layer model in the context of microelectrode voltammetry was assessed by recording the ratio of the current under conditions of constant ultrasonic irradiation (I_{sono}, recorded at 44 W cm^{-2}) to that found under silent conditions (I_{silent}). This was modelled using the theory given above and a best fit value of z^* inferred. Note that by using the ratio I_{sono}/I_{silent} the dependence on D and a_{bulk} is removed. Figure 16 shows the dependence of z^* on the electrode radius in the form of a plot of log (z^*) against log (r_e). Also included

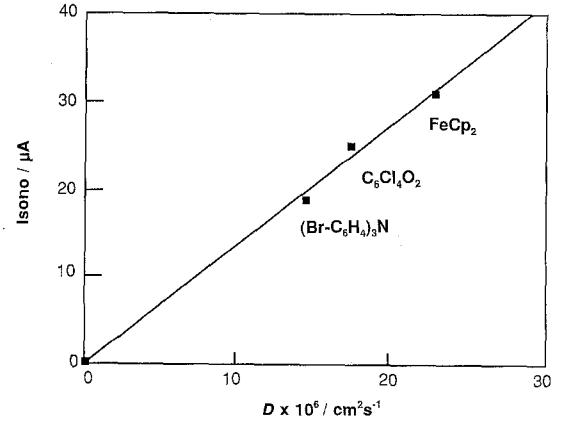

Fig. 13. Plot showing that the current observed at a sonicated macroelectrode depends on diffusion coefficient of the electroactive species as predicted by Equation 3. In each experiment a concentration of 10^{-3} M of the depolarizer was used. The electrode size was 0.05 cm and the ultrasonic power was 44 W cm^{-2}.

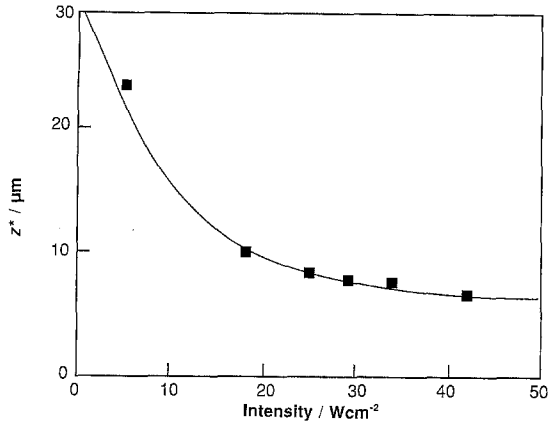

Fig. 14. Variation of the diffusion layer thickness with the intensity of incident ultrasonic power at macroelectrodes of radius of 0.39 cm, as inferred from the voltammetry of Cp_2Fe.

on the figure are the values of z^* reported in Table 1. It can be seen that at low radii the effective diffusion layer thickness tends to the $(1/r_e)$ dependence expected for unperturbed mass transport to a microdisc electrode and implicit in Equation 2. Under these conditions, at sufficiently small electrodes,

$$I_{sono} \longrightarrow I_{silent}$$

Notice for large radii electrodes the diffusion layer thickness tends to a fixed, power dependent value as noted above.

The results summarized in Fig. 16 vindicate the theoretical approach proposed earlier in this paper. As a further check on the conceptual basis underpinning our work ac impedance spectroscopy was carried out using macroelectrodes with the ferrocene system. A frequency range between 0.1 Hz and 65 kHz was investigated with the electrode potential held at a value close to that of the halfwave potential of the Cp_2Fe/Cp_2Fe^+ system. The resulting data was displayed in the form of Nyquist plots in which the imaginary and real components of the impedance are displayed. Figure 17 shows the Warburgian behaviour [22] expected for a reversible electrode couple (in the absence of insonation) under conditions of semiinfinite diffusion. The equation describing this

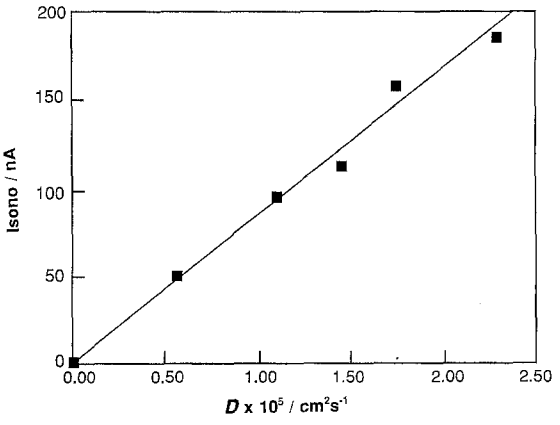

Fig. 15. Variation of the steady state electrode current with diffusion coefficient of the electroactive species for a microelectrode of radius 30 μm and an incident power of 44 W cm^{-2}.

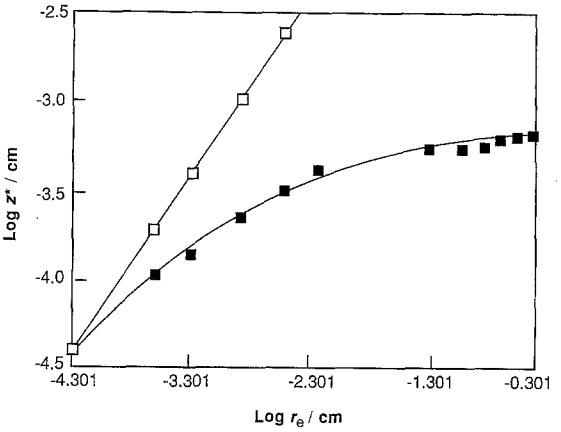

Fig. 16. Dependence of z^* on electrode radius. The values of z^* were inferred from voltammetric measurements made on the Cp_2Fe system. The straight line asymptote drawn for small values of r is the average diffusion layer thickness, $z^* = \pi r_e/4$, deduced from Equation 2 which relates to unperturbed mass transport to a microdisc electrode. Key: (■) sono/experimental; (□) silent theory (microdiscs only).

response is

$$Z(\omega) = R_u + \frac{4RT\cosh^2(\theta/2)}{n^2F^2A\omega^{0.5}D^{0.5}a_{bulk}}\frac{(1-j)}{\sqrt{2}} \qquad (6)$$

where n is the number of electrons transferred, ω/rad s^{-1} is the a.c. frequency, $\theta = nF/RT(E - E^0)$ (where E is the electrode potential and E^0 is the standard potential) and R_u is the uncompensated solution resistance. Equation 6 shows that a plot of the negative value of the component of the imaginary impedance ($-Z''$) against $1/\sqrt{\omega}$ should be a straight line through the origin as confirmed by Fig. 18. The slope of this plot enabled the inference of a value of $2.5(\pm 0.2) \times 10^{-5}$ cm^2 s^{-1} for the diffusion coefficient of Cp_2Fe which is in good agreement with literature values of 2.3×10^{-5} cm^2 s^{-1} [11, 18]. Figure 19 reveals the corresponding Nyquist plot made for the same electrode as used to generate the data needed for Fig. 17 except that the electrode was irradiated with ultrasound of power 44 W cm^{-2}. Notice that the impedance is greatly reduced owing to the enhanced mass transport and that the shape of the impedance plot is qualitatively altered. We have suggested above

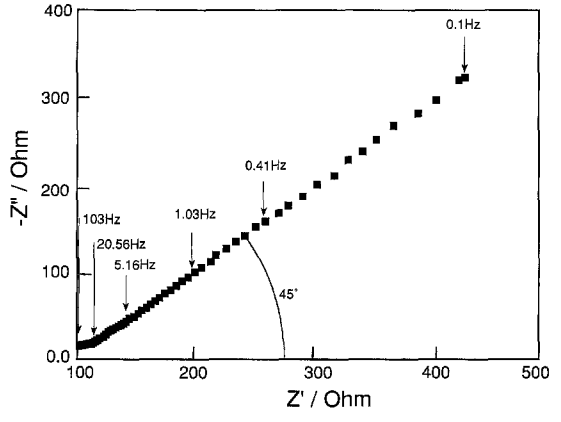

Fig. 17. Nyquist plot showing the imaginary ($-Z''$) and real (Z') components of impedance as measured using an electrode of radius 0.39 cm and a solution of Cp_2Fe (10^{-3} M) in acetonitrile/0.1 M TBAP.

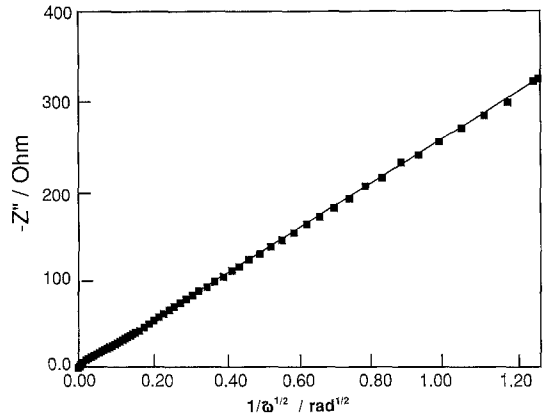

Fig. 18. Plot of $-Z''$ against $1/\sqrt{\omega}$ derived from Equation 6, the plot gradient enables the determination of D for Cp_2Fe.

that for macroelectrodes under sonication the mass transport is controlled by diffusion through a thin film. For such conditions it is readily shown [23, 24] that the Warburg expression of Equation 6 should be replaced by the following:

$$Z(\omega) = R_u + \frac{4RT\cosh^2(\theta/2)}{n^2F^2Aa_{bulk}D^{0.5}\omega^{0.5}\sqrt{2}}(1-j) \times \tanh(z^*\sqrt{(j\omega/D)}) \quad (7)$$

Equation 7 was applied to our experimental data and z^* systematically varied to obtain the best fit with experiment. The results of this procedure are shown in Fig. 19. In addition Fig. 20 shows the corresponding exercise applied to an electrode of radius 0.30 cm. For both electrodes examined it can be seen that the diffusion layer thickness indirectly inferred from the a.c. impedance measurements is in close agreement with those reported in Table 1 with the best fits in both cases being seen for z^* values between 5 and 7 μm in good agreement with the values of 6.5 μm shown in Table 1 above.

As a final confirmation current transients were recorded when induced by a leap between potentials corresponding to no current flow and to the transport

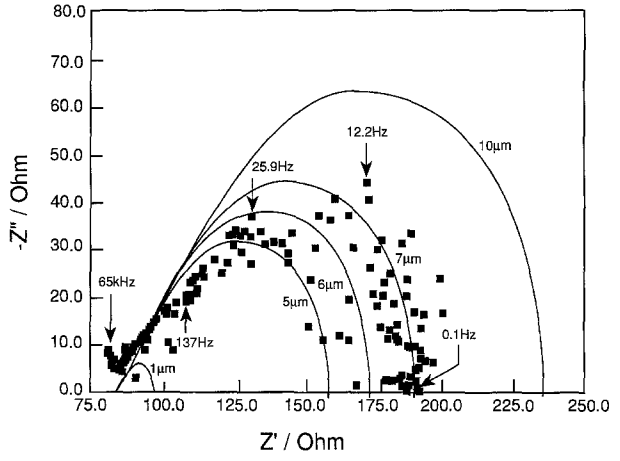

Fig. 19. Nyquist plot showing imaginary $(-Z'')$ and real (Z') components of the impedance as measured in the presence of ultrasound (20 kHz, 44 W cm^{-2}) using an electrode of radius 0.39 cm and a solution of Cp_2Fe (1 mM) in acetonitrile/0.1 M TBAP. Solid lines represent the theoretical behaviour computed from Equation 7 for the values of z^* shown.

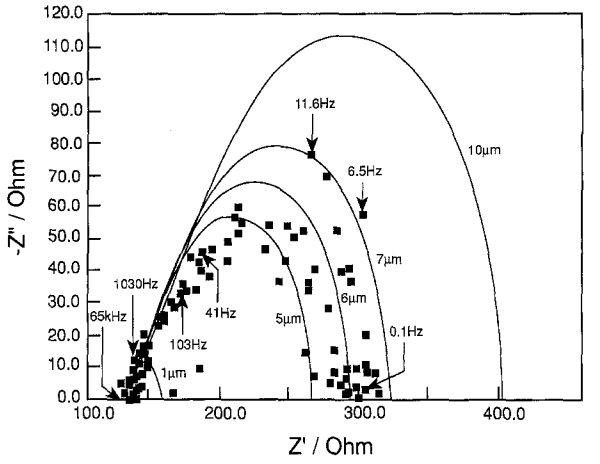

Fig. 20. Nyquist plot showing imaginary $(-Z'')$ and real (Z') components of impedance as measured in the presence of ultrasound (20 kHz, 44 W cm^{-2}) using an electrode of radius 0.30 cm and a solution of Cp_2Fe (1 mM) in acetonitrile/0.1 M TBAP. Solid lines represent the theoretical behaviour computed from Equation 7 for the values of z^* shown.

limited oxidation of ferrocene at a 29 μm microdisc electrode. Figure 21 shows transients recorded both in the absence and presence of ultrasound. Both were quantitatively modelled using the Hopscotch

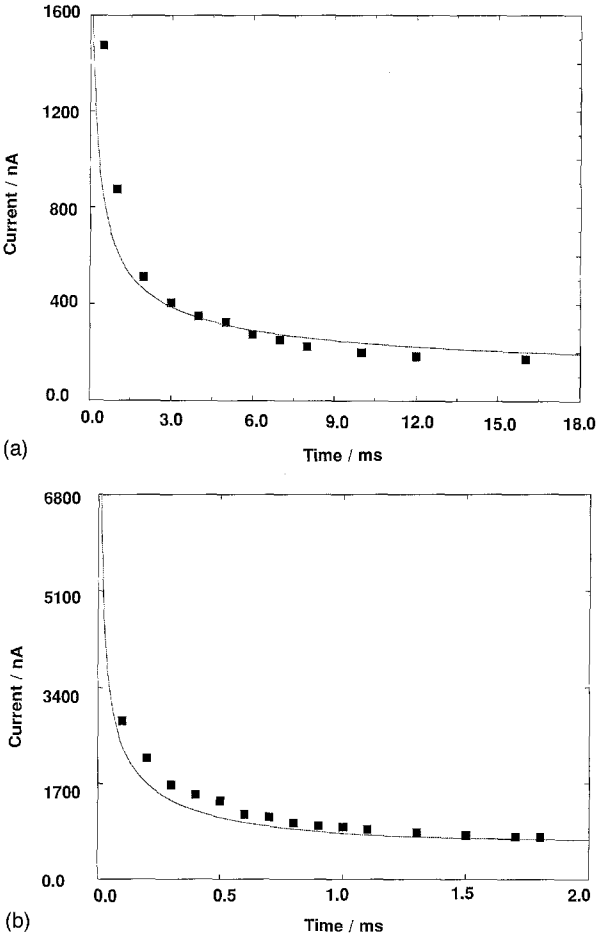

Fig. 21. Potential leap transients recorded for the oxidation of Cp_2Fe (3.2 mM) at a 29 μm microdisc electrode (a) in the absence of ultrasound, and (b) with the electrode irradiated by ultrasound of power 55 W cm^{-2}. Points correspond to experimental measurements; solid line corresponds to theoretically predicted response computed using the truncated diffusion layer model described in the test. A layer thickness of 3.1 μm was used for the computations as deduced from analysis of the steady state current.

theory given above. In the presence of ultrasound the diffusion layer thickness (3.1 μm) deduced from the steady state current was used in the computations. The excellent agreement between theory and experiment shown in Fig. 21 again confirms our proposed mass transport model.

6. Conclusions

Steady-state voltammetry, a.c. impedance spectroscopy and potential step chronamperometry all suggest that the mass transport to an electrode (microelectrode or millielectrode) under conditions of insonation may be characterized by transport across a thin diffusion layer of thickness about a few tens of nanometres and which is dependent on the power of the ultrasound employed. It should be emphasized that the measurements reported are on a timescale long compared to a single cavitational event and therefore represent an averaged response of the electrode; the response of an electrode at short times, comparable to those of the ultrasound frequency used, may reveal different behaviour.

Acknowledgements

We thank EPSRC for a studentship for JCE and Zeneca (Fine Chemical Manufacturing Organisation) for the loan of their W380 ultrasonic horn and the EC for financial support (contract no. CHRX CT94 0475) under the Human Capital and Mobility Scheme.

References

[1] R. Walker, *Chem. Britain* **26** (1990) 251.
[2] B. Brown and J. E. Goodman, 'High Intensity Ultrasonics', Iliffe Books (1965).
[3] U. Akbulut, L. Toppare and K. Yurrtas, *Polymer* **27** (1986) 803.
[4] S. Oswana, M. Ito, K. Tanaka and J. Kuwano, *Synth. Met.* **18** (1987) 145.
[5] T. J. Mason, J. P. Lorimer and D. J. Walton, *Ultrasonics* **28** (1990) 333.
[6] J. Kilma, C. Bernand and C. Degrand, *J. Electroanal. Chem.* **367** (1994) 297.
[7] D. J. Walton, S. S. Phull, A. Chyla, J. P. Lorimer, T. J. Mason, L. D. Burre, M. Murphy, R. G. Compton, J. C. Eklund and S. D. Page, *J. Appl. Electrochem*, in press.
[8] D. Shoup and A. Szabo, *J. Electroanal. Chem.* **140** (1982) 237.
[9] *Idem, ibid.* **160** (1984) 17.
[10] A. M. Bond, K. B. Oldham and C. G. Zoski, *ibid.* **245** (1988) 71.
[11] R. G. Compton, A. C. Fisher, R. G. Wellington, P. J. Dobson and P. A. Leigh, *J. Phys. Chem.* **97** (1993) 10410.
[12] R. G. Compton, R. A. W. Dryfe, J. A. Alden, N. V. Rees, P. J. Dobson and P. A. Leigh, *ibid.* **98** (1994) 1270.
[13] J. Heinze, *J. Electroanal. Chem.* **124** (1981) 73.
[14] R. G. Compton, B. A. Coles, M. B. G. Pilkington and D. Bethell, *J. Chem. Soc. Faraday Trans. 1* **86** (1990) 663.
[15] A. M. Bond, A. G. Wedd, J. B. Cooper and D. M. Way, *Inorg. Chem.* **32** (1993) 2416.
[16] R. G. Compton, J. Booth, J. C. Eklund, S. G. Davies, W. C. Wadkins and M. R. Metzler, *J. Chem. Soc. Perkin Trans. II.* (1993) 1603.
[17] P. Sharp, *Electrochim Acta.* **28** (1983) 301.
[18] M. Fleischmann and S. Pons, 'Ultramicroelectrodes', Datatech, Morganton, NC (1987).
[19] Yu. S. Gerasimenko, M. A. Gerasimenko and L.I. Antropov, *J. Electroanal. Chem.* **63** (1975) 275.
[20] 'Handbook of Chemistry and Physics', 55th edn, Weast CRC Press (1974–5).
[21] E. T. Seo, R. F. Nelson, J. M. Fritsch, L. S. Marcoux, D. W. Leedy and R. N. Adams, *J. Am. Chem. Soc.* **88** (1966) 3498.
[22] M. Peover, *J. Chem. Soc.* (1962) 4540.
[23] A. J. Bard and L. R. Faulkner, 'Electrochemical Methods', J. Wiley & Sons, New York (1980).
[24] Southampton Electrochemistry Group, 'Instrumental Methods in Electrochemistry', Ellis Horwood, Chichester (1985).